Magnetic Porous Carbon from Biomass for Malachite Green Removal

Yichun Wu *

Nanjing Foreign Language School, Nanjing, 210018, China

* Corresponding author: mmabe51632@student.napavalley.edu

Abstract. For years, environment protection, especially how to purify industrial and agricultural wastewater, has been a disputable issue. The scarcity of water resources increases the urgency of wastewater recycling. Meanwhile, emitting wastewater into rivers and farmland deteriorated environmental issues. To solve this problem, a low-cost and efficient way to produce porous carbon which can adsorb organic solute and then be removed is being discussed in this report, aiming to separate organic pollutants from wastewater. In this report, ferric chloride, potassium carbonate, and biomass (like sawdust) are used to fabricate porous carbon. These ingredients all low-cost and easy to be found in usual laboratory, suggesting that it is simple to imitate this method. Porous carbon produced in this method has excellent specific surface area of 1517 m^2/g, which has an adsorption capacity for MG (malachite green) aqueous solution of 988.6 mg/g in maximum.

Keywords: Porous carbon, adsorption, malachite green, biomass.

1. Introduction

Activated carbon, a specialized form of carbon derived from organic sources like fruit shells, coal, and wood, has extensive historical use in water purification. This material undergoes a meticulous transformation involving heating these organic materials in air-isolated conditions to eliminate non-carbon components, known as carbonization. Subsequently, it's exposed to gases to erode the surface and form a microporous structure, termed activation. The activation process is inherently microscopic, where numerous molecular carbide surfaces undergo point erosion, resulting in activated carbon with a vast array of minuscule pores [1, 2]. The application in the report is based on this character of activated carbon.

K_2CO_3 decomposes at high temperatures to produce high amounts of gas and is often used as a pore-making material in the carbonization process to reach high adsorption capacity. As the sample is heated in the tube furnace, K_2CO_3 is thermally decomposed to produce carbon dioxide. CO_2 forms pores in the sample, similar to the principle of fermentation [3]. Ferric ion dissociated from $FeCl_3$ are converted under high-temperature heating to different types of ferric oxides, of which only Fe0, Fe_3O_4 and γ-Fe_2O_3 are magnetic. This method allows carbonization and magnetization to occur simultaneously in the tube furnace while heating under a nitrogen environment [4].

Malachite green, with the molecular formula $C_{23}H_{25}ClN_2$, is a synthetic organic compound, a toxic triphenylmethane chemical that is both a dye and a fungicide, bactericide, and parasiticide, and can be carcinogenic when used in excess over a long period of time. MG is effective against water mold of fish body and eggs. Now there is no special drugs on the market can cure the water mold disease for a short period of time, which is the fundamental reason the aquaculture industry farmers quite risky to continue to ignore the national ban on the use of MG. In order to cope with the problem of purifying agricultural wastewater, MG was chosen for this study as an adsorption application of the produced carbon sample [5, 6].

Firstly, this report describes the fabrication process of the porous carbon. Then, the data analysis of the four samples are presented. Finally, the adsorption capacity for MG was explored.

2. Materials and Methods

2.1. Preparation

In all four samples, a mixture consisting of 100 ml of deionized water, 10 g of biomass, and 2 g of anhydrous $FeCl_3$ was employed as the base. To vary the potassium carbonate (K_2CO_3) and biomass ratio, weight ratios of 0, 0.5, 1, and 2 were used. These mixtures were vigorously shaken at 150 rpm for 4 hours, followed by drying at 353 K in an air environment for 18 hours. After drying, the biomass was ground and subsequently activated at 973 K for 2 hours under a nitrogen (N_2) flow of 1 L/min, with a heating rate of 4 K/min. Subsequently, the carbonized sample underwent two washes with diluted hydrochloric acid (HCl, 2 M) and deionized water. Finally, it was dried again at 353 K for 18 hours. Four samples are denoted as S-0, S-0.5, S-1, S-2, where the number are weight ratios of K_2CO_3 to biomass. The samples were then subjected to Brunauer–Emmett–Teller (BET), elemental, Brunauer–Emmett–Teller (FTIR), X-Ray Diffraction (XRD), Vibrating Sample Magnetometer (VSM), and Raman tests, respectively.

2.2. Adsorption of Malachite Green

The two samples with the lowest and highest K_2CO_3 to biomass weight ratios, 0 and 2, respectively, were selected as control experiments. Next, solutions with different MG concentrations were configured, where the carbonized samples were all at a concentration of 1 g/L. In the solutions with samples to which the weight ratio of K_2CO_3 to biomass was 0, the concentrations of MG were 100, 50, 25, 12.5, 5, 1 mg/L; in the solutions with samples to which the weight ratio of K_2CO_3 to biomass was 2, the concentrations of MG were 1000, 800, 500, 300, 200, 100, 50, 10 mg/L. Meanwhile, MG solution at concentrations of 50, 25, 10, 5, 2, 1 mg/L were configured to confirm the standard curve. Two copies of each concentration of the solution were configured for replication of the experiment. The samples were then vigorously shaken (150 rpm) for more than 18 h so that MG could be fully adsorbed. Finally, the filtered samples were sequentially tested for residual MG concentration by infrared spectrophotometer.

3. Results and Discussion

3.1. Textual Properties of Carbon Composites

K_2CO_3, acted as a porogen, had a significant effect on increasing the surface area of the carbon composites. The lowest surface area, that of the unadded K_2CO_3 sample, was only 583 m^2/g. As a comparison, the S-1 sample with the highest surface area amounted to 1517, nearly three times that of the S-0 sample. The data in Table 1 demonstrated the excellent pore-making ability of K_2CO_3. As shown in Table 2, the more K_2CO_3 added, the smaller the yield, indicating the most of K_2CO_3 decomposed at high temperatures to produce gases that escaped. Meanwhile, the data in Table 1 show that the sample with the most K_2CO_3 added was not the one with the largest surface area, although the difference was not significant. That is, at the same temperature, the gas produced by about 10 g of K_2CO_3 was already at the limit. Adding too much would instead shift the equilibrium in the opposite direction, causing less gas to be produced. Fig. 1 also proved this point. S-1 sample had the highest adsorption isotherm, suggesting that the optimal amount of K_2CO_3 added in this research is 10 g. However, shown in Table 1, the microporosity (V_{mic}/V_t) increased while the K_2CO_3 impregnation ratio increased.

Table 1. Surface Area, Pore Volume and Pore Size

0	S_{BET} (m^2/g)	S_{mic} (m^2/g)	S_{mic}/S_{BET} (%)	V_t (cm^3/g)	V_{mic} (cm^3/g)	V_{mic}/V_t (%)	pore size (d, nm)
S-0	583	529	90.7	0.306	0.209	68.3	2.10
S-0.5	1265	1207	95.4	0.605	0.470	77.7	1.91
S-1	1517	1439	94.9	0.713	0.561	78.7	1.88
S-2	1455	1388	95.4	0.674	0.537	79.7	1.85

Table 2. Yields and Elemental Compositions

sample	yield (%)	C (%)	N (%)	S (%)	O (%)
S-0	24.0	85.95	0.22	0.11	12.64
S-0.5	12.6	76.55	0.71	0.11	21.76
S-1	10.3	66.19	1.45	0.10	31.09
S-2	7.2	71.23	0.94	0.15	26.86

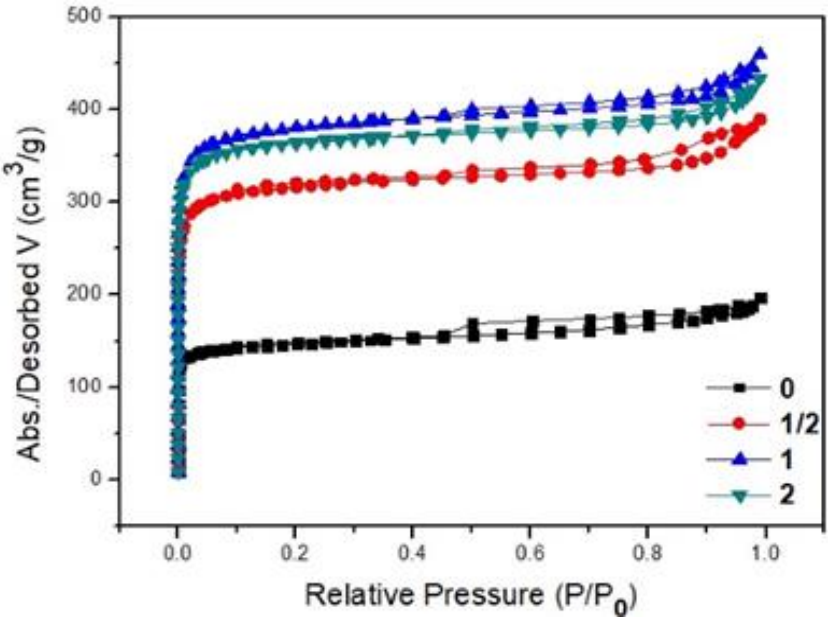

Figure 1. Adsorption-Desorption Isotherms of N_2. (Picture credit: Original)

Fig. 2 shows that most of the pore size distributions are in the range of 0.5 to 2.0 nm; Fig. 1 showed that all four adsorption isotherms were type I isotherms. Both analyses confirmed that the carbon composites predominantly featured micropores (pore size < 2 nm), aligning with Table 1 data. Notably, Fig. 1 highlighted a substantially greater total pore volume for S-0.5, S-1, and S-2 compared to S-0. Additionally, average pore size of four samples shown in Table 1 indicated that it was related with the amount of K_2CO_3 added. The average pore size decreased while the amount of K_2CO_3 increased, also suggesting the existence of more micropores. Because of the pore-filling effect, micropores adsorb organic matter better than mesopores, which further demonstrated the importance of K_2CO_3.

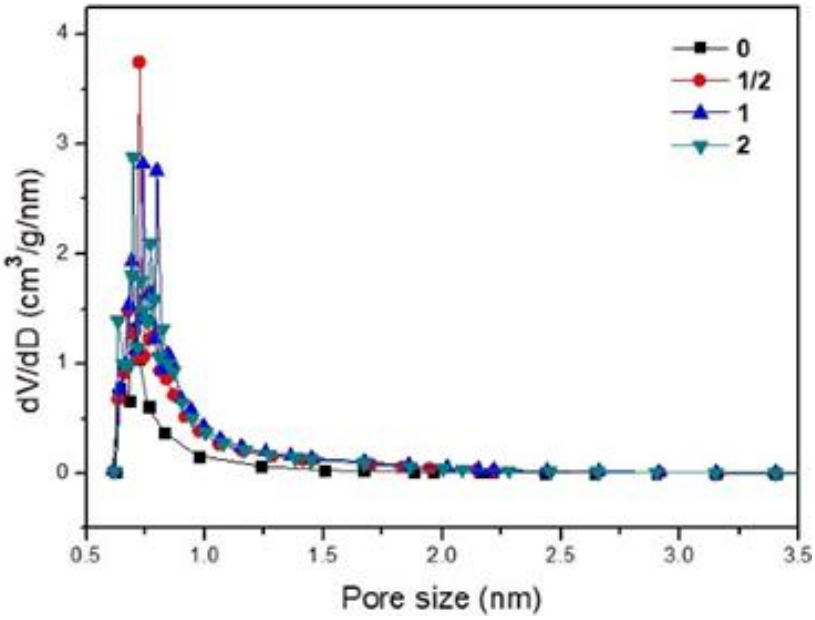

Figure 2. Pore Size Distribution. (Picture credit: Original)

3.2. Magnetic Properties

Fig. 3 displayed the XRD patterns of the carbon composites, revealing a peak at 2θ = 26.4˚, corresponding to (002) of the graphitized carbon, indicating the presence of graphitic layers [7]. It can also be seen that the highest degree of graphitization is the lowest addition of K_2CO_3.

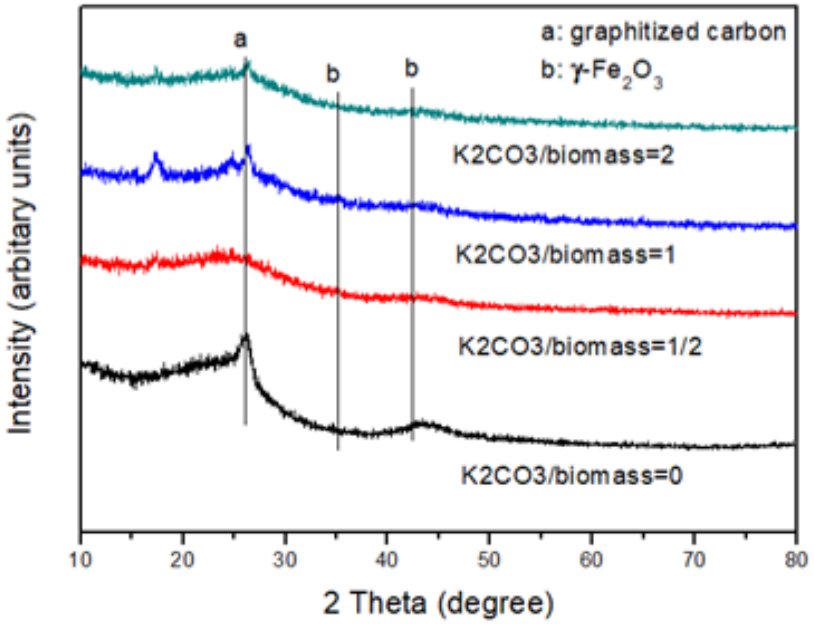

Figure 3. XRD patterns of the carbon composites. (Picture credit: Original)

The b-peak noted at 2θ = 35.3˚ and 42.9 ˚ corresponds to the Fe_3O_4/γ-Fe_2O_3 lattice. Fe_3O_4 and γ-Fe_2O_3 lattice perform the same in the XRD pattern. Equations (1)-(3) shows the conversion of $FeCl_3$ (ferric ions) to Fe_3O_4/γ-Fe_2O_3 [8].

$$FeCl_3 + 2H_2O \rightarrow FeOCl \cdot H_2O + 2HCl \rightarrow FeOOH + 3HCl \text{ (473-673 K)} \quad (1)$$

$$2FeOOH \rightarrow \gamma\text{-}Fe_2O_3 + H_2O \text{ (673-703 K)} \quad (2)$$

$$Fe_2O_3 + C \rightarrow Fe^0 + CO \quad (3)$$

From Fig. 3, it can be seen that the b-peak is very weak, indicating that all four samples do not contain high levels of Fe_3O_4/γ-Fe_2O_3. It may be that because of the high surface area of the carbon composites, the Fe^0 on the surface was washed away. As shown in the third equation, carbon may react with Fe_2O_3, and then produced CO gas that escaped. This fact could echo with the diminishing yields as the K_2CO_3 impregnation increased. Fig. 4 is the Raman spectra of the carbon composites.

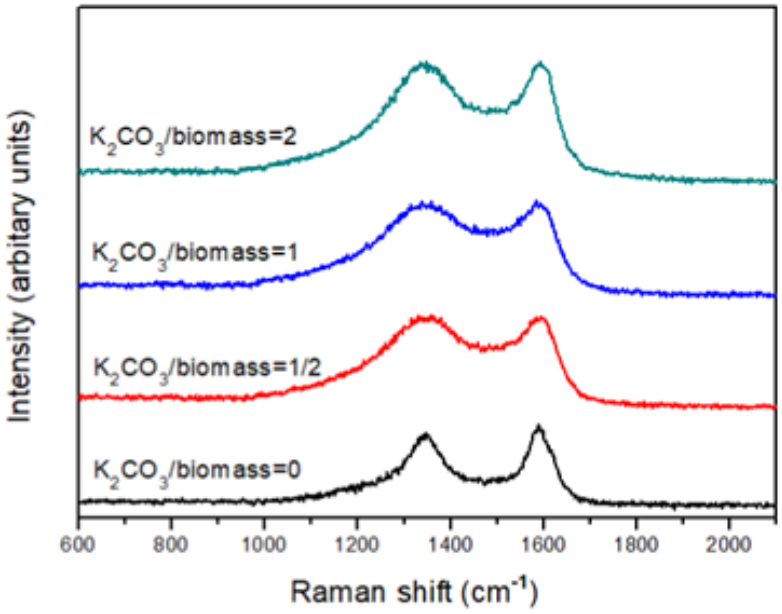

Figure 4. Raman spectra of the carbon composites. (Picture credit: Original)

Fig. 5 shows the FTIR spectra of the carbon composites. The carbon composites have oxygen groups included ester, hydroxyl, ether, alcohol and phenol groups. It is noteworthy that there are two peaks at 589 cm^{-1} and 642 cm^{-1}, which are mainly attributed to vibrations of Fe-O. Fe-O may originate from tetrahedral and octahedral sites in the spinel structure. Due to the existence of Fe_3O_4/γ-Fe_2O_3 particles and carbon matrix, these two peaks confirmed the formation of C-O-Fe bonds [4].

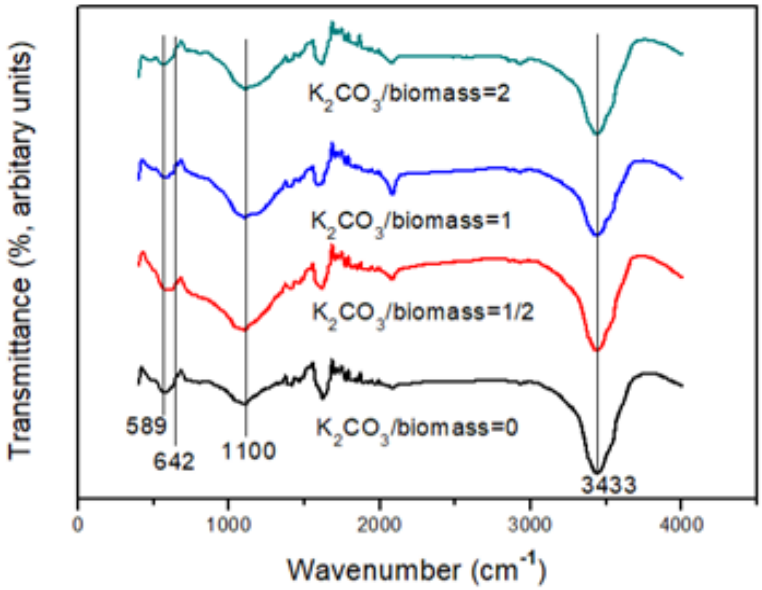

Figure 5. FTIR spectra of the carbon composites. (Picture credit: Original)

The weakness of the intensities suggests that the Fe_3O_4/γ-Fe_2O_3 particles were wrapped by partially graphitized carbon powder, which is proved by XRD analysis [9, 10]. Meanwhile, the amount of K_2CO_3 added had made slightly difference on the intensity.

Fig. 6 shows the hysteresis loop of the carbon composites. It can be seen that the loop is reversible and nonlinear. The magnetization is in the range of -0.15~+0.15 emu/g, indicating that the magnetism

of the carbon composites is quite weak. As mentioned earlier, it is possible that the Fe_3O_4/γ-Fe_2O_3 transferred into Fe^0 while heated under high temperatures. Subsequently the Fe^0 was washed away, resulting in weak magnetism.

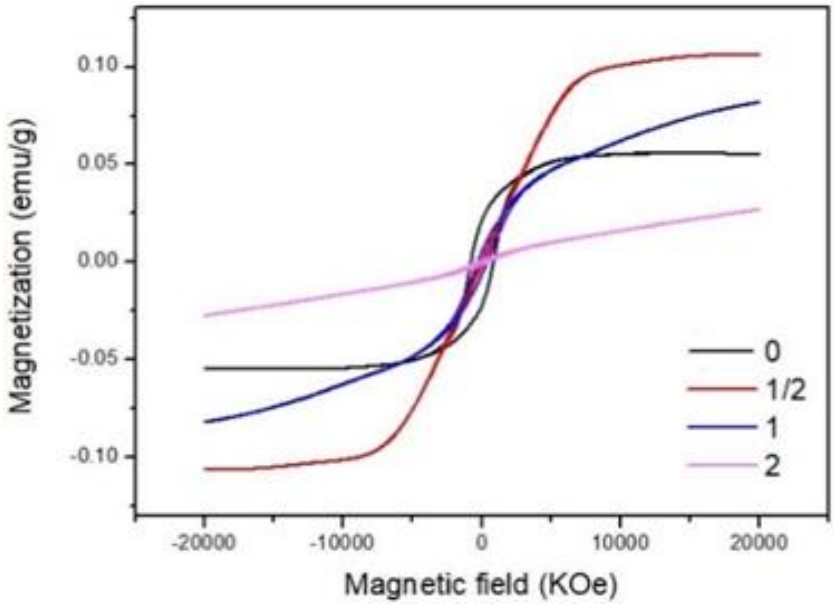

Figure 6. Hysteresis loop of the carbon composites. (Picture credit: Original)

3.3. Adsorption Performance of MG

The greater the material's pore count and surface area, the higher its adsorption capacity due to the pore-filling effect. In this section, the S-0 and S-2 samples were used to study their adsorption, and both samples were selected based on initial surface area predictions. Fig, 7 visualizes the comparison of the solution concentration after adsorption, showing that the maximum adsorbed concentration of the S-2 carbon composites has reached 988.6 mg/L and that of the S-0 composites has only reached 49.4 mg/L. The huge differences in the adsorption concentrations of S-0 and S-2 carbon composites also corroborate the differences in their surface areas and pore volumes.

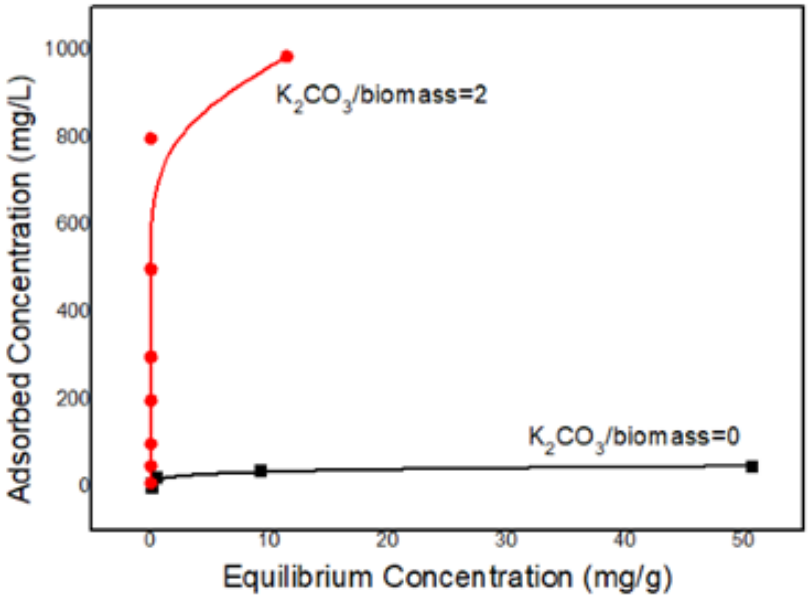

Figure 7. MG adsorption isothermal folds. (Picture credit: Original)

The adsorption data of MG was fitted to the Langmuir model: [4]

$C_e/q_e = 1/ bq_m + C_e/q_m$

Where C_e (mg/L) is the equilibrium concentration of the MG, q_e (mg/g) is the equilibrium adsorption capacity, b (L/mg) is the Langmuir constant, and q_m (mg/g) is the maximum adsorption capacity.

As shown in Fig. 8, the adsorption data fits the Langmuir model well, with the $R^2 = 0.99 > 0.95$. The results showed that the S-2 sample, to which 20 g of K_2CO_3 was added, had an excellent adsorption capacity for MG. On the maximum point, $C_e/q_e = 988.6$ mg/g, which means that 1 g of the carbon composites can adsorb 988.6 mg of MG solute. Fig. 9 is MG adsorption Langmuir fitting of S-0. Fig.10 is MG adsorption Langmuir fitting of S-2

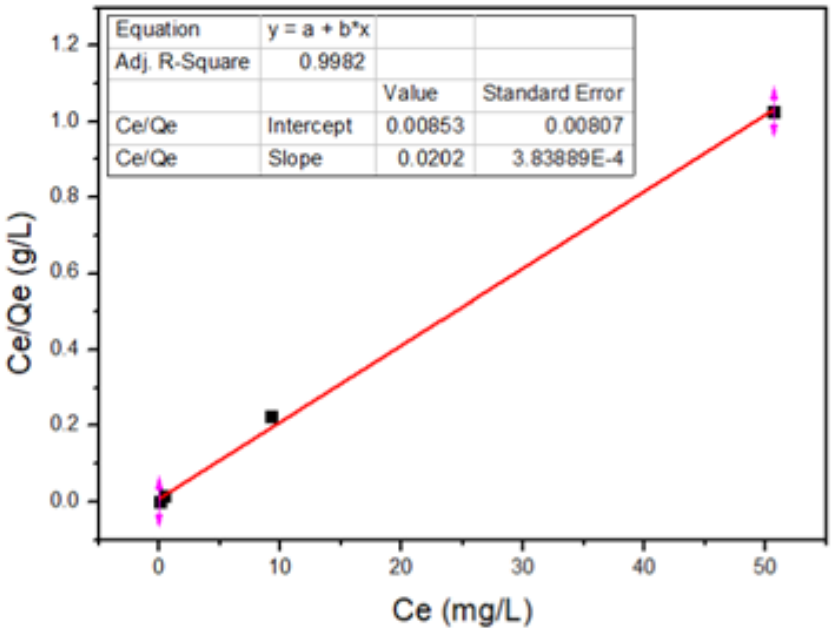

Figure 8. MG adsorption linear fitting of S-0. (Picture credit: Original)

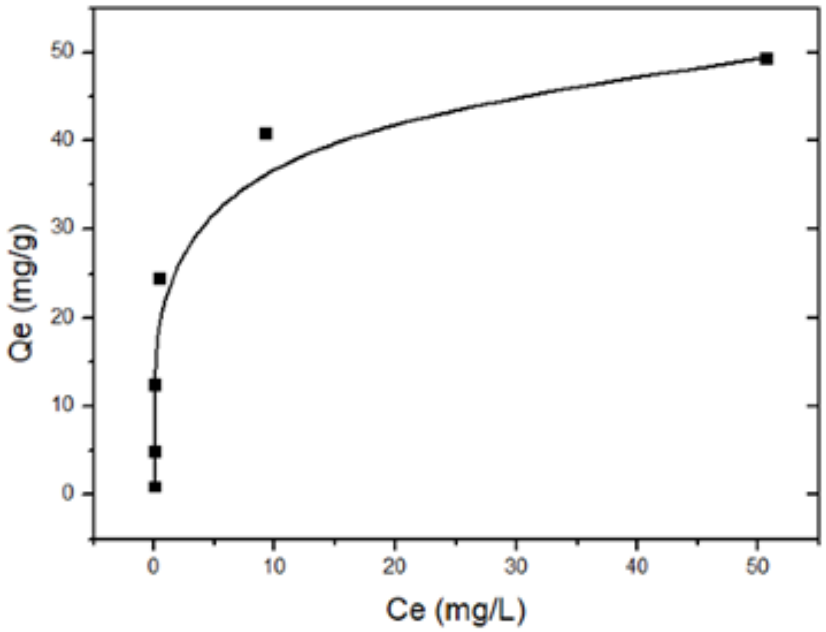

Figure 9. MG adsorption Langmuir fitting of S-0. (Picture credit: Original)

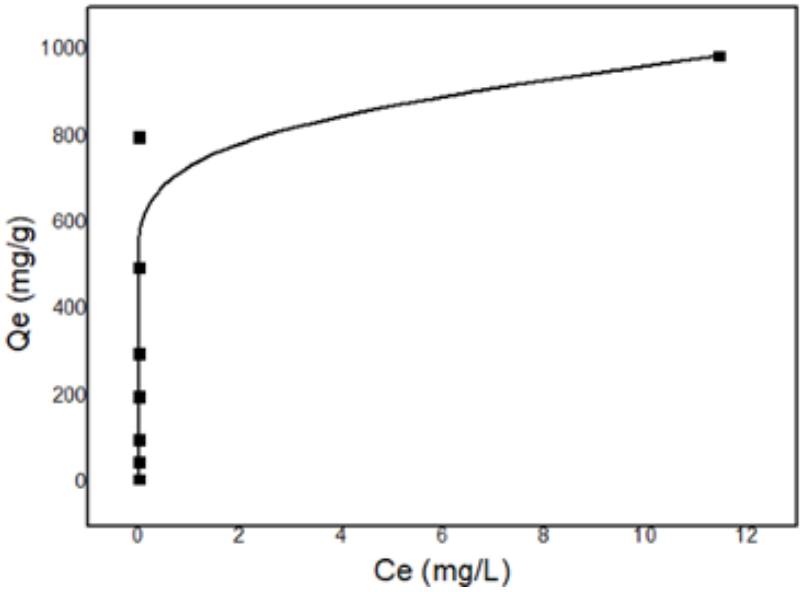

Figure 10. MG adsorption Langmuir fitting of S-2. (Picture credit: Original)

Organic pollutants adsorption is promoted by the high surface area and pore volumes. In Table 2, S-1 stands out as the sample boasting the highest surface area and pore volume, so 988.6 mg/g is not the limit for this carbon composites.

4. Conclusion

Adsorption of organic pollutants with activated carbon composites is quite an effective way to purify industrial and agricultural wastewater. Not only does this method not create excess impurities in the water, but it is also inexpensive and simple to produced. K_2CO_3 greatly increases the surface area of the carbon and forms a large number of micropores which play the main role in absorption due to the micropore-filling effect, leading to a high absorption capacity of the carbon composites. In the subsequent studies, both the amount of K_2CO_3 and the activation temperature will be controlled separately as single variables to investigate which temperature and K_2CO_3 impregnation ratio will give the carbon composites the highest surface area and the strongest magnetic properties.

References

[1] Zhang Y., Application of activated carbon adsorption in industrial wastewater treatment. Coal and Chemical Industry, 2011, 34 (6): 74 - 76.

[2] Polovina M., Babic B., Kaluderovic B., Dekanski A., Surface characterization of oxidized activated carbon cloth. Carbon, 1997, 35 (8): 1047 – 1052.

[3] Wei Y., Zhou, J., Yang L., Gu J., Chen Z., He X., N/S co-doped interconnected porous carbon nanosheets as high-performance supercapacitor electrode materials. New Carbon Materials, 2022, 37 (4): 707 - 715.

[4] Xiang Z., Liu Y., Luo G., Qian F., Zhang S., Chen J., Facile Fabrication of Magnetic Carbon Composites from Hydrochar via Simultaneous Activation and Magnetization for Triclosan Adsorption. Environmental Science and Technology 2014, 48: 5840 - 5848.

[5] Adina R., Alexandra O., Mihaela P., Dumitru O., Influence of surfactants on the fading of malachite green, Central European Journal of Chemistry, 2008, 6: 1895 – 1066.

[6] Babendure R., Adams R., Tsien Y., Aptamers Switch on Fluorescence of Triphenylmethane Dyes. Journal of the American Chemical Society. American Chemical Society (ACS). 2003, 125 (48): 14716 – 14717.

[7] Li Y., Zhu C., Lu T., Guo Z., Zhang D., Ma J., Zhu S., Simple fabrication of a Fe2O3 /carbon composite for use in a high-performance lithium-ion battery. Carbon 2013, 52: 565 − 573.

[8] Rufford T.E., Hulicova-Jurcakova D., Zhu Z., Qing L., A comparative study of chemical treatment by FeCl3, MgCl2, and ZnCl2 on microstructure, surface chemistry, and double-layer capacitance of carbons from waste biomass. J. Mater. Res. 2010, 25: 1451 − 1459.

[9] Keiluweit M., Nico P. S., Johnson M.G., Kleber M., Dynamic molecular structure of plant biomass-derived black carbon (biochar). Environ. Sci. Technol. 2010, 44: 1247 − 1253.

[10] Zhu H. Y., Jiang R., Xiao L., Zeng G.M., Preparation, characterization, adsorption kinetics and thermodynamics of novel magnetic chitosan enwrapping nanosized γ-Fe2O3 and multi-walled carbon nanotubes with enhanced adsorption properties for methyl orange. Bioresour. Technol. 2010, 101: 5063 − 5069.